



A01-16748

**AIAA 2001-0944**  
**Simulation of Combustion Driven**  
**Micro-Engine**

M. Kirtas and S. Menon  
*School of Aerospace Engineering*  
*Georgia Institute of Technology*  
*Atlanta, GA 30332*

**39th AIAA Aerospace Sciences**  
**Meeting and Exhibit**  
**January 8-11, 2001/Reno, NV**

# Simulation of Combustion Driven Micro-Engine

M. Kirtas\* and S. Menon†  
*School of Aerospace Engineering*  
*Georgia Institute of Technology*  
*Atlanta, GA 30332*

A numerical study of a combustion driven micro-engine is presented in this paper. There are some unique issues in the design of this engine due to the dimensions of the combustor and since Micro Electro-Mechanical Systems (MEMS) fabrication technology has to be used in its manufacture. Phenomena such as ignition, flame propagation, heat losses and quenching may occur differently due to the small size of the device, especially the high aspect ratio of the combustor. Since these effects control the performance of the engine, an in-depth parametric evaluation is necessary to develop an optimal successful design. However, due to the MEMS fabrication limitations, parametric experimental studies is not only difficult but also very expensive. To complement an on-going experimental effort and to reduce the design cycle costs, a large-eddy simulation (LES) methodology has been developed to carry out the aforementioned parametric studies in a more cost-effective manner and to provide guidelines for the construction of the micro-engine. The simulation results are compared with available experimental data and results show reasonable agreement. The relevance and importance of various parameters of the micro-engine is then discussed and implications for design are highlighted.

## Introduction

A free piston engine is a device that employs combustion to establish into cyclic motion a piston that is then used to directly produce energy. There are many successful designs of this device and some of their key features were summarized on a recent survey.<sup>1</sup> In general, a free piston engine can be used to generate hydraulic, pneumatic or electrical energy and past designs have employed either a single piston or an opposed or dual piston setup depending on the position of the combustion chamber(s) and piston(s). The relevance of several design parameters, such as the fuel injection timing, energy conversion efficiency, sealing and losses have been discussed earlier<sup>1</sup> in the context of past designs. Some of these issues will be re-addressed in the present study. In another recent study<sup>2</sup> the application of free piston configuration with opposed combustors was discussed as a device for generating electrical energy. They presented results for a "Benchtop Model" where the emphasis was on obtaining the experimental pressure versus volume diagram since this type of information can give simple order of magnitude estimate of the efficiency of power conversion.

The various free-piston engines discussed in the above noted papers were of dimensions that were small but not necessarily considered an extreme limit. Recently, with the advent of MEMS technology application to practical systems, there has been considerable interest in investigating systems that are either

very small (i.e., micron-scale) or devices that require MEMS fabrication technology in order to build the device. Micro-engines that employ both these approaches are being investigated. An example of a MEMS-scale engine is the micro-turbine being developed at MIT,<sup>3</sup> whereas a device that is small enough to require MEMS fabrication technology is currently being developed at Georgia Tech.<sup>4</sup> A key feature of all these designs is the need to demonstrate a very small device capable of producing appreciable energy (e.g., 10-30 Watts of electrical power) in order to be useful for practical application. Of special interest in the present study is a device that employs fluidic power, i.e., combustion, to drive the generator to obtain electric power. Compared to conventional power sources, MEMS manufactured generators will have a high power density and a relatively long life. As a result, such a device may find many applications both in military and civilian fields. For example, an application of key interest to the US Army is the ability to provide portable power for the systems a soldier must carry. Thus, a system independent "soldier" power pack could have many applications.

A device under development at Georgia Tech incorporates a free piston located between two opposed combustors. This piston is set into motion due to out-of-phase combustion in the two opposed combustors. To generate electric power from this device, the entire assembly is confined inside a magnet array. The interaction of the magnetic field with the piston motion generates the required electric energy. A schematic of this device is shown in Fig. 1. Note that, the actual scale of the entire device (including the magnetic array) is no larger than a pack of playing cards.

\*Graduate Student

†Associate Fellow, AIAA

Copyright © 2001 by M. Kirtas and S. Menon. Published by the American Institute of Aeronautics and Astronautics, Inc. with permission.

Although the above device is conceptually sound, the aforementioned problems regarding achieving cyclically consistent and accurate injection, mixing, ignition and combustion within a very small combustor (in order to generate sustained steady-state electric power) requires significant optimization of the design of the device. Key parameters include the location of the inflow and outflow ports, the timing of the opening and closing of these ports, and control of leakage and heat transfer loss from the system. The various problems associated with optimizing these parameters has led the experimental effort to a more simplified configuration in which the engine consists of a single combustor with the other combustor replaced by a spring that provides a pre-defined force to mimic the "phantom" combustor. A similar device is numerically simulated in the present paper using LES.

In the following sections we describe the methodology used for LES, the problems addressed in this paper and the results obtained. It is to be noted that to the authors' knowledge this is the first attempt to simulate a free piston combustion system using LES. Furthermore, the results of the present LES effort is being used to provide guidelines for the hardware construction. Therefore, this effort provides an unique demonstration of the ability and the use of LES results for practical design of complex systems.

## Governing Equations for LES

The governing equations of motion are the usual Navier-Stokes equations for a general compressible, reacting flow. Spatial Favre filtering of the governing equations using a suitable (top hat) filtering operator along with the decomposition of the flow field into a subgrid (unresolved) and supergrid (resolved) parts results in a set of conservation equations for the resolved properties. Unknown terms in these equations representing the contribution of the unresolved subgrid quantities have to be modeled. The final set of LES equations are:

$$\frac{\partial \bar{\rho}}{\partial t} + \frac{\partial}{\partial x_i} [\bar{\rho} \tilde{u}_i] = 0 \quad (1)$$

$$\frac{\partial \bar{\rho} \tilde{u}_i}{\partial t} + \frac{\partial}{\partial x_j} [\bar{\rho} \tilde{u}_i \tilde{u}_j + \bar{p} \delta_{ij} - \bar{\tau}_{ij} + \tau_{ij}^{sgs}] = 0 \quad (2)$$

$$\frac{\partial \bar{\rho} \tilde{E}}{\partial t} + \frac{\partial}{\partial x_i} [(\bar{\rho} \tilde{E} + \bar{p}) \tilde{u}_i + \bar{q}_i - \tilde{u}_j \bar{\tau}_{ji} + H_i^{sgs} + \sigma_{ij}^{sgs}] = 0 \quad (3)$$

$$\frac{\partial \bar{\rho} \tilde{Y}_m}{\partial t} + \frac{\partial}{\partial x_i} \left[ \bar{\rho} \tilde{Y}_m \tilde{u}_i - \bar{\rho} \tilde{D}_m \frac{\partial \tilde{Y}_m}{\partial x_i} + \Phi_{i,m}^{sgs} + \theta_{i,m}^{sgs} \right] = \bar{w}_m \quad (4)$$

for  $m = 1, N$

### Subgrid Closure

There are many terms in the above equations that appear due to the filtering process and must be closed. The unclosed terms  $\tau_{ij}^{sgs}$ ,  $H_i^{sgs}$ ,  $\sigma_{ij}^{sgs}$ ,  $\Phi_{i,m}^{sgs}$ , and  $\theta_{i,m}^{sgs}$

represent the subgrid stress tensor, subgrid heat flux, subgrid viscous work, species mass flux and species diffusive mass flux, respectively. These terms have been described in detail elsewhere<sup>5-7</sup> and therefore, only a brief description will be given here. In the present formulation, closure of the subgrid stress terms is achieved using a transport model for the subgrid kinetic energy per unit mass  $k^{sgs} = \frac{1}{2} [\tilde{u}_k^2 - \bar{u}_k^2]$ :

$$\frac{\partial \bar{\rho} k^{sgs}}{\partial t} + \frac{\partial}{\partial x_i} (\bar{\rho} \tilde{u}_i k^{sgs}) = P^{sgs} - D^{sgs} + \frac{\partial}{\partial x_i} \left( \bar{\rho} \frac{\nu_t}{Pr_t} \frac{\partial k^{sgs}}{\partial x_i} \right) \quad (5)$$

where  $P^{sgs} = -\tau_{ij}^{sgs} \frac{\partial \tilde{u}_i}{\partial x_j}$  and  $D^{sgs} = C_\epsilon \bar{\rho} (k^{sgs})^{3/2} / \bar{\Delta}$  are the production and dissipation terms, respectively.

Subgrid stress tensor is closed by using an eddy viscosity hypothesis based on the subgrid turbulent kinetic energy. Thus,  $\tau_{ij}^{sgs} = -2\bar{\rho} \nu_t (\tilde{S}_{ij} - \frac{1}{3} \tilde{S}_{kk} \delta_{ij}) + \frac{2}{3} \bar{\rho} k^{sgs} \delta_{ij}$ , where the eddy viscosity is  $\nu_t = C_\nu (k^{sgs})^{1/2} \bar{\Delta}$ . Here,  $\bar{\Delta}$  is the filter width which is related to the local grid size. There are two coefficients  $C_\nu$  and  $C_\epsilon$  in this model that have to be specified. A localized dynamic approach to determine these coefficients have been developed and shown to be robust in complex flows.<sup>7</sup> However, for the present effort, using results from a recent study,<sup>8</sup> the coefficients  $C_\nu$  and  $C_\epsilon$  are taken as 0.067 and 0.916, respectively. Dynamic modeling will be carried out in the near future.

Subgrid heat flux and species subgrid mass flux terms follow similar definitions based on gradient diffusion model and are given by

$$H_i^{sgs} = -\bar{\rho} \frac{\nu_t}{Pr_t} \frac{\partial \tilde{h}}{\partial x_i} \quad (6)$$

and

$$\Phi_{i,m}^{sgs} = -\bar{\rho} \frac{\nu_t}{Sc_t} \frac{\partial \tilde{Y}_m}{\partial x_i} \quad (7)$$

where the turbulent Prandtl number and Schmidt number are chosen as 0.9 and 0.92, respectively.  $\tilde{h}$  is the mixture enthalpy. Subgrid diffusive mass flux term  $\theta_{i,m}^{sgs}$  is neglected since it is shown to be relatively small compared to the subgrid species mass flux  $\Phi_{i,m}^{sgs}$ . Finally, the subgrid viscous work is modeled as

$$\sigma_{ij}^{sgs} = C_\epsilon \bar{\rho} (k^{sgs})^{3/2} \quad (8)$$

### Reaction Rate Closure

Premixed methane-air combustion is studied in the present effort. For the initial study, a global, single step finite-rate kinetics model is employed. For LES applications, the closure of the reaction rate is somewhat problematic and has been the focus of many recent efforts. In general, the filtered reaction rate can be computed (a) by assuming the joint scalar probability density function (PDF),<sup>9</sup> (b) by solving for

the subgrid PDF<sup>10,11</sup> or (c) by employing a simplified algebraic relation such as Eddy Break-Up (EBU) or Eddy Dissipation Concept (EDC). Spalding<sup>12</sup> proposed the first EBU model for computing mean reaction rate of fuel in a turbulent flow. This model has been used with some minor changes for both premixed and non-premixed combustion. Several variants of the model have since appeared in the literature and it has been shown also that in the limit of very fast chemistry, presumed PDF methods can be cast into EBU type relations.<sup>13</sup> In this study, the closure of the mean reaction rate is obtained by employing a modified break-up model EBU<sup>14</sup> where the interaction of small scale structures with the large eddies is modeled by determining the time scale at which reactions take place. For chemistry, a global decomposition reaction of the form  $R \rightarrow P$  for a premixed mixture of  $CH_4$  and air is employed. The Arrhenius type reaction rate expression is  $w_R = \rho Y_R A \exp(-T_a/T)$  where  $A = 5.55 \times 10^9$  1/sec and  $T_a = 14786$  K.<sup>15</sup> The filtered reaction rate is then determined as

$$\bar{w} = [(\bar{w}^{mass})^{-1} + (\bar{w}^{chem})^{-1}]^{-1} \quad (9)$$

where  $\bar{w}^{chem}$  is the chemical reaction rate (obtained from the Arrhenius expression above) and  $\bar{w}^{mass}$  is the mass destruction rate due to mixing which is given by

$$\bar{w}^{mass} = (\bar{\rho} \tau_M^{-1}) \min\{\tilde{Y}_m [-(v_m^P - v_m^R) M_m]^{-1}\} \quad (10)$$

Here,  $\tau_M = (1 - \gamma)/\dot{m}$  is a characteristic mixing time scale. In this formulation,<sup>14</sup> the mass transfer per unit mass per unit time between fine structures and the surrounding fluid is defined as  $\dot{m} = (\frac{5}{16} \xi^{-2})^{1/4} (\varepsilon \nu)^{1/4}$ . Finally, the intermittency of this process is modeled through the intermittency factor  $\gamma = (125 \xi^2)^{1/4} \lambda_{sgs}^{-1} (\nu^3 / \xi)^{1/4}$ . Here,  $\xi = 0.09$  and  $\varepsilon = k^{3/2} / \bar{\Delta}$  and  $\nu$  is the usual kinematic viscosity. The relevant information leading to this formulation can be found elsewhere.<sup>14</sup> Using the above relations, the filtered reaction rate for each species can be written as:

$$\bar{w}_m = M_m \sum_m (v_m^P - v_m^R) \bar{w} \quad (11)$$

The above approach, although an approximation, is computationally very cost effective and is considered sufficient for a first attempt to demonstrate a design level LES approach. An alternate and more accurate method would be to use a subgrid scalar evolution model such as the subgrid linear-eddy model approach developed earlier.<sup>8,11</sup> The need for such a complex and relatively more expensive modeling approach will be evaluated later depending upon the ability of the present model to provide design level results of acceptable accuracy.

## The Micro-Engine

During the course of this study, a series of engine designs were investigated. Initially, in both the experiments<sup>4</sup> and numerical efforts<sup>16,17</sup> the dual combustor configuration similar to Fig. 1 were studied. Figure 2 shows a schematic of the device simulated numerically. For parametric studies, different options of this device were also investigated. Figure 3 shows four such designs which differed primarily in the location(s) of the inflow and outflow ports. The rationale behind these designs and some of the pertinent results (which were reported earlier<sup>16,17</sup>) are summarized in the Results section.

The current research effort is focused on a simpler device and a planform view of the engine is given in Fig. 4. This design was chosen for the experimental effort to address some problems related to achieving cyclic combustion in the dual system and to understand the dynamics of the process. Typical dimensions and parameters for this experimental device are summarized in Table 1 (these values were also used for the LES studies reported here). The free piston engine has two scavenging ports one of which is also used for inflow of premixed reactants. In a typical cycle of combustion, there are three phases: an intake phase, a combustion phase and an exhaust phase. In the experiments, the injection is at an angle from one of the ports to the wall where reactants will eventually be ignited. A similar approach is employed in the LES. Ideally, the injection angle should be varied to determine the ideal inclination that will give a mixture as uniform as possible after the intake phase. This is an issue to be addressed once the present model has been validated using the existing experimental data.

The intake phase is a continuous one, in other words, if the pressure in the chamber is below a predetermined value then injection of the reactants will occur provided that the ports are open. During the intake phase, pre-compression occurs and before the piston reaches TDC (Top Dead Center), ignition occurs. The ignition time is of the order of 0.2 msec. After ignition, flame propagation, volumetric expansion and pressure rise effects causes the piston to move back to Bottom Dead Center (BDC) which is the end of one cycle. Note that, there is no outside interference to control the opening and closing of the ports. Rather, the opening and closing of the ports is done automatically by the moving piston itself. Thus, piston, during its motion, acts as an actuating mechanism so that, depending on the position of the piston, the ports might be open or closed. This is important design consideration for this engine because other means of controlling the state of the ports will require supplementary mechanism(s). Integration of such a control mechanism in a small device will increase the complexity and drive up the cost and therefore, is to be avoided.

Since the piston motion controls the status of the

ports (i.e., open/closed) it can effect a variety of things, such as the maximum pressure obtained, the concentration of the unburned reactants just before the exhaust ports opens, the amount of burnt products remaining, etc., and through these effects directly impact the oscillatory state of the combustion process and the frequency of oscillation. The frequency of oscillation directly controls the power generated by this device and therefore, achieving a fixed frequency is critical for the success of this design. Hence, for a given fuel mixture, the ports should be at a location (relative to ignition zone) such that combustion is completed before the exhaust phase. This point is closely linked to other phenomena such as the turbulence level in the combustor during combustion and quenching especially near the walls. The latter has particular importance in the present context since the combustor has very small spanwise dimension and the flame will reach the lateral walls before it reaches the other walls.

### Numerical Issues

The conservation equations are solved using a finite-volume scheme with a predictor-corrector time-stepping. This scheme is second order accurate both in space and time. No-slip boundary conditions are applied on all walls for the velocity field. Since unsteady heat transfer to the wall has been identified as an important factor in the experimental studies, a time-dependent heat flux boundary condition is employed during some stage of the combustion process as described later. For simplicity, mass loss from the domain in-between the piston and the wall is neglected. The retarding force due to the magnetic coils is also not considered. These issues will be addressed in a future study. Thus, the present form of the simulated problem is a pure combustion problem with moving boundaries. Figures 2 and 4 show the combustors along with the appropriate dimensions. Notice that the spanwise dimension is much smaller than the other two directions and thus, this device has a very high aspect ratio. To properly resolve this domain, a computational grid of  $191 \times 101 \times 13$  is used and for this resolution the grid size is about  $0.5mm$  in all directions. Thus, a uniform grid resolution is used in the present effort to avoid any grid stretching errors. Earlier studies addressed the issue of grid resolution and it was determined that for this combustion problem, such a resolution is sufficient to resolve the flame zone.

Inflow conditions are specified using characteristic inflow conditions.<sup>18</sup> Randomly generated turbulent fluctuations is added to the inflow velocity and subgrid kinetic energy is also specified at the inflow. Typical values used here are taken from Tabaczynski.<sup>19</sup> The exit pressure is specified at the outflow and all other variables are extrapolated from the interior.

To move the piston, a simple force balance between

the fluidic force (obtained by multiplying the average pressure in the chamber by the frontal area of the piston) and the opposing spring force is employed. Spring details are given in Table 1. This procedure takes into account some of the inertial effects. Thus, the momentum of the piston is not neglected. Note that in the real system the spring is not attached to the piston and the spring exerts a force which is a linear function of displacement. At top dead center (TDC), the spring is already displaced  $5.1\text{ mm}$  ( $0.2\text{ in}$ ). Since the time scale of integration is on the order of  $10^{-7}\text{ sec}$ , the corresponding piston motion is very small. In order to reduce the computational effort, the piston is not moved in the computational domain at every time step but rather, the computed displacements are summed in time till it reaches a reasonable fraction of the grid size before the piston is moved. More specifically, a displacement based on velocity increments is computed by  $\sum F \times \Delta t = M \times \Delta V$  where  $\sum F$  and  $\Delta V$  are the total force acting on the piston and the velocity increment at each time step, respectively. Here,  $M$  is the piston mass. The total force is equal to the difference between the average pressure in the chamber and the piston force that can be calculated by Hooke's Law. Then, the piston is moved when the summed displacements exceed the local grid size. Thus, the displacement, if any, is on the order of the local grid size. Furthermore, no rotational effects about the center of gravity of the piston due to local chamber pressure variations are considered for the present.

### Results and Discussions

Results of the present effort are summarized in this paper. Initial studies of ignition in a constant volume combustor was carried out to determine the importance of heat transfer to the wall on the effective pressure rise in the combustor. Subsequently, both two-dimensional (2D) and three-dimensional (3D) LES studies of the dual-combustor micro-engines (Fig. 2) were carried out and compared to determine if 2D studies (which are computationally very cost effective) can be used with reasonable accuracy for parametric evaluation of various designs. Finally, the experimental device (Fig. 4) is simulated in 3D to investigate the nature of oscillation and to obtain data for comparison. Discussion of the sensitivity and applicability of the LES results is then carried out.

#### Effect of Wall Heat Transfer

To determine the impact of wall heat transfer, 2D and 3D simulations were carried out using adiabatic and unsteady heat flux at the wall using a constant volume combustor. In this case, the combustor volume was  $4225 (50 \times 13 \times 6.5)mm^3$  and a resolution of  $100 \times 60$  and  $100 \times 60 \times 10$  were used for 2D and 3D respectively. This case corresponds to a case that was experimentally investigated in the past. Details of this

study was reported elsewhere.<sup>16,17</sup> Fig. 5 summarizes the results of this study. It can be seen that both 2D and 3D calculations reproduce the pressure rise with reasonable agreement. Furthermore, the effect of wall heat transfer is dramatic and results in a significant drop in the peak pressure. This is an important issue for the design of this device since the pressure rise directly translates into the motion of the piston which in turn determines the power output from this device. Thus, for an optimal design, reduction in wall heat transfer should lead in a more efficient design. However, practical manufacturing problems and the types of material available for MEMS fabrication may place an upper limit on the control of the amount of heat transfer through the walls. This implies that wall heat transfer must be included in all modeling studies. Ideally, for proper modeling, the heat conduction problem through the physical walls must be solved along with the LES flow problem in the combustor. These issues will be considered in a follow-on study.

Although comparison with data shows reasonable agreement for the heat transfer case, there are some discrepancies especially in the initial stages. This is related to the differences in the ignition process used in the experiment and in the model. In the experiments, multiple spark sources were employed whereas in the simulation a small volume in the domain was preheated. Thus, the initial flame kernel formation and its growth are quite different. Numerically, it is very difficult to mimic the spark ignition process. Furthermore, there could be other reasons that could result in the observed differences, for example, the use of global chemistry in the model, the effect of flame growth and quenching near the walls which is not modeled, etc. Again, these issues are being addressed and will be reported in the near future.

### Dual-Combustor Micro-Engine

As noted earlier, there were problems in the fabrication and operation of this engine in the early stage of this project. In fact, one of the earlier design failed to maintain the oscillation and would stop after couple of oscillations. Since it was difficult to determine from the actual device what was happening inside the combustor, a series of numerical studies were carried out to determine the reasons. Four different configurations were studied. Figure 3 shows these configurations and they differ primarily in the location of the inflow and outflow ports. Results of these studies were reported earlier<sup>17</sup> and therefore, only key highlights are summarized here. Some of these designs had a fundamental problem, namely that the reactant concentration in the chamber could not be increased to a level sufficient to sustain combustion. This is shown in Fig. 6 which shows the reactant concentration reached during the injection phase and before the outflow is opened. Ideally, the concentration should reach unity as quickly

as possible. It can be seen that Designs 3 and 4 were successful while Designs 1 and 2 failed to achieve high reactant concentration in the chamber before ignition. As a result, the Designs 1 and 2 does not maintain sustained oscillation. Note that, Design 1 is very similar to the earlier experimental device.

To determine why this design failed the flow field was analyzed. It was determined that in this case, some of the burnt products gets trapped in the combustor and effects the inflow of the reactants. In fact, due to this trapped products, some of the reactants escape through the outflow port before ignition. Representative velocity vector fields for Design-1 and for Design-4 (which was successful) are shown in Fig. 7. Note that, for the failed Design-1 case, burned products are trapped in the top and bottom corners (marked by symbol B) and some of the reactants (marked by a symbol R) actually escape through the outflow port before it is closed. In contrast, Design-4 due to the location of the outflow port allows all the burned products to exit while the injected reactant is still filling the chamber.

Simulations such as this are quite useful in obtaining quick answers to the modifications to the design since construction of this device would have taken a long time. Furthermore, the above studies were also conducted using both 2D and 3D codes to see if there is any similarity in the flow field. It was determined from the numerical studies that 2D and 3D simulations reproduce very similar process and the predicted pressure amplitude and frequency were very close. This is shown in Fig. 8. This is important since 2D simulations are computationally very inexpensive and therefore, a large number of parametric simulations can be carried out quickly in order to obtain some quick answers. On the other hand, for a more realistic combustion process, the effect of small-scale turbulence (which is 3D) needs to be included. Therefore, eventually, full 3D simulations are necessary to investigate the final design.

### Single-Combustor Micro-Engine

The earlier study established the numerical methodology and demonstrated its ability to capture some of the dynamics of the flow field. The dual-combustor studies showed how a successful design could be achieved. However, designs such as Design-4 required additional mechanism to open and close the ports (since they were located further from the piston). From an experimental point of view a more simpler design was preferred and this resulted in the aforementioned development of the single-combustor design.

The single combustor model is designed with simplicity in mind and provides one with more control over the relevant parameters. Recently some experimental results has been reported,<sup>4</sup> mainly for pressure history and position of the piston. So far, three combustors

of different size have been experimentally studied<sup>4</sup> but only one with chamber thickness of  $6.25\text{mm}$  is simulated here. Experimentally, this combustor achieved sustained oscillation as described below.

Experimental pressure and position history are given in Fig. 9. Corresponding numerical solution is also shown in Fig. 9. General trends are captured well in the numerical solution. The predicted frequency (43 Hz) is close to the measured value (32 Hz) and the peak pressure is also close and differs by less than 10%. There are, however, some differences as well. The ignition in the numerical solution is somewhat slower which in turn impact the combustion process. As noted earlier, the ignition process used in experiments (multiple spark plugs) is very difficult to mimic in the numerical approach and therefore, some discrepancy in the initial period is expected. In the real configuration, as can be seen in Fig. 9, combustion is almost finished at TDC, which explains the relatively higher peak pressure obtained. On the other hand, in the numerical simulation (Fig. 9) combustion continues even after TDC. There could be various reasons for this difference. For example, it may be a consequence of the limitation of the EBU reaction rate closure model that is employed here which will impact the chemical conversion rate. Additionally, the magnitude of inflow turbulence (which in turn can effect the mixing time scale) could impact this result. At present, there are no measurements in the combustor to determine some of these quantities and therefore, additional simulations with different conditions may be necessary to determine the difference.

Another observation is that the experimental pressure begins to decrease long before the ports are open and as a result, the  $P - V$  experimental diagram is both qualitatively and quantitatively different than the computed  $P - V$  diagram. These figures are shown in Fig. 10a and 10b, respectively. This difference can be attributed to heat and mass losses observed in the experiments (and which are not currently included in the model) and the model for the spring constant for the simulation. At present, there is no quantified information available from the experiments for these parameters and other parameters such as retarding force due to the generator, etc., and one has to resort to guessing their values. For example, the experimental value of the spring constant  $k = 1183.3\text{N/m}$  was not sufficient in the simulation phenomena such as the losses and retarding force were unaccounted. We resorted to including their effect by increasing the spring constant in an ad hoc manner. To determine the sensitivity of the simulations to the choice of the spring constant, two simulations were carried out using different values of the spring constants:  $k = 2081\text{N/m}$  and  $k = 2381\text{N/m}$  (as shown above). Increasing the spring constant slightly increases the peak pressure and the stroke length of the piston but the frequency is al-

most unchanged. Higher spring constant give more time near TDC and this explains the slight pressure increase. On the other hand, it also accelerates the return to TDC from BDC, thus tending to compensate for frequency. These result suggests that more information from the experimental device is needed to fully model all the features in this device.

It should be noted that although the spring constant was increased above the experimental value to model for the missing effects, it still gives a linear response in space. However, the neglected factors may all contribute to nonlinearity to a certain degree and therefore, without further quantified information from the experiments (which is likely to be nearly impossible), it will be very difficult to exactly match the data. Nevertheless, the present simulations have been able to reproduce nearly all the dynamical features observed in the experiments and also provided a new capability that can be utilized (at least in an idealized manner) to study such devices. Such a capability can be very useful for optimizing the final design of the micro-engine.

Figures 11 and 12 show respectively, the subgrid kinetic energy and temperature at ignition and injection phase. It can be seen that in both phases there is a significant amount of subgrid kinetic energy in the domain. Especially during injection, significant fluctuations are occurring in the high shear region of the injected jet. Spanwise views show that there is also significant three-dimensionality in the domain suggesting that for this configuration (which involves an angled, high-speed injection), full 3D simulations may be necessary to understand the dynamics of the mixing and combustion process.

Finally, the experimental frequency is close to 32 Hertz while either of the numerical solutions is about 43 Hertz. According to Zinn et al.,<sup>4</sup> a free piston device in the frequency range 25 – 50 Hertz will produce about 20 W electrical power. This is within the design goal of this project.

## Conclusions

A LES methodology has been developed to simulate combustion process in a free piston micro-engine. Simulations have been carried out for various design configurations in order to understand the dynamics of the combustion process in high aspect ratio combustors. The simulation results have been used to identify critical design issues and to provide guideline for the manufacture of this engine. These studies form the first such reported application of LES to hardware design and provide confidence on the ability of LES predictions. Comparison of the LES predictions with available data show reasonable agreement. In particular, the dynamics of sustained oscillation has been captured well although there are some differences in the actual values. However, as noted above,

there are many uncertainties in the experimental device that cannot be quantified and hence, cannot be modeled properly. Nevertheless, the LES model has shown its potential for addressing these flows in a more cost-effective manner and therefore, may become an important tool in the design of micro-engines in the near future.

Future studies of this micro-engine will address system parameters that are critical for optimizing the performance of the engine. Heat conduction through the wall will be included to model more accurately the heat transfer effect. The impact of injection strategy (orientation, location, port size, etc.) will also be addressed. Finally, further effort will be directed towards determining a model to include heat losses in a more accurate manner.

### Acknowledgments

This work was supported by Army Research Office and DARPA under a Multidisciplinary University Research Initiative.

### References

<sup>1</sup>Achten, A. J. P., "A Review of Free Piston Engine Concepts," ASME Paper 941776, 1994.

<sup>2</sup>Clark, N. N. and Famouri, P., "Modeling and Development of a Linear Engine," ASME Paper 98-ICE-95, 1998, In 1998 Spring Technical Conference, ICE-Vol. 30-2.

<sup>3</sup>Waitz, I. A., "Combustors for micro-gas turbine engines," *Journal of Fluids Engineering*, Vol. 120, No. 1, 1998, pp. 109-117.

<sup>4</sup>Zinn, B. T., Glezer, A., and Allen, M. G., "Model and Sub-component Development for a Pulse-Combustion-Driven Micro-generator," Tech. rep., Sept. 1999, Report to DARPA/ARO.

<sup>5</sup>Menon, S., Yeung, P. K., and Kim, W. W., "Effect of subgrid models on the computed interscale energy transfer in isotropic turbulence," *Computers and fluids*, Vol. 25, No. 2, 1996, pp. 165-180.

<sup>6</sup>Kim, W. W. and Menon, S., "LES of Turbulent Fuel-Air mixing in a Swirling Combustor," AIAA Paper 98-0200.

<sup>7</sup>Kim, W. W., M. S. and Mongia, H. C., "Large-Eddy simulation of a gas turbine combustor flow," *Combustion Science and Technology*, Vol. 143, 1999, pp. 25-62.

<sup>8</sup>Chakravarthy, V. K. and Menon, S., "Large Eddy Simulations of Turbulent Premixed Flames in the Flamelet Regime," *Combustion Science and Technology*, 2000, to appear.

<sup>9</sup>Borghì, R., "Turbulent Combustion Modelling," *Prog. Energy Combust. Sci.*, Vol. 14, 1988, pp. 245-292.

<sup>10</sup>Chakravarthy, V. K. and Menon, S., "Subgrid modeling of premixed flames in the flamelet regime," *Flow, Turbulence and Combustion*, 2000, to appear.

<sup>11</sup>Menon, S., "Subgrid combustion modelling for large-eddy simulations," *Int. J. Engine Research.*, Vol. 1, No. 2, 2000, pp. 209-227.

<sup>12</sup>Spalding, D. B., "Mixing and Chemical Reaction in Steady Confined Turbulent Flames," *Thirteenth Symposium (International) on Combustion*, The Combustion Institute, 1971, pp. 649-657.

<sup>13</sup>Bray, K. N. C. and Moss, J. B., "A unified statistical model of premixed turbulent flames," *Acta astronaut.*, Vol. 4, No. 3-4, 1977, pp. 291-319.

<sup>14</sup>Pureby, C. and Moller, S.-I., "Large Eddy Simulation of Reacting Flows Applied to Bluff Body Stabilized Flames," *AIAA Journal*, Vol. 33, No. 12, 1995, pp. 2339-2347.

<sup>15</sup>Westbrook, C. K. and Dryer, F. L., "Simplified Reaction Mechanisms for the Oxidation of Hydrocarbon Fuels in Flames," *Combustion Science and Technology*, Vol. 27, 1981, pp. 31-43.

<sup>16</sup>Rabindra, N. P., Kapoor, R., Kim, J. H., and Menon, S., "Simulation of Combustion-Driven Micro Power Generator," Dec. 1999, Poster presentation, 28th Symposium (international) on Combustion.

<sup>17</sup>Rabindra, N. P., Kapoor, R., Kim, J. H., and Menon, S., "Combustion Dynamics in a Compact Power Generator," *The 8th Conference (International) on Numerical Combustion*, Amelia Island, Florida, 2000.

<sup>18</sup>Poinsot, T. J. and Lele, S. K., "Boundary Conditions for Direct Simulations of Compressible Viscous Flows," *J. Comput. Phys.*, Vol. 101, 1992, pp. 104-129.

<sup>19</sup>Tabaczynski, R. J., "Turbulence and Turbulent Combustion in Spark-Ignition Engines," *Prog. Energy Combust. Sci.*, Vol. 2, 1976, pp. 143-165.

**Table 1 Engine description**

• single piston against an opposing spring
• two stroke engine
• combustion system: premixed
• piston stroke: ~ 4.3cm
• piston mass: 0.1 kg
• flow rate: 17.75 m <sup>3</sup> /hour
• spring constant: 1183.3 N/m
• chamber dimensions(in cm):
6.00 × 5.0 × 0.625 at BDC
1.70 × 5.0 × 0.625 at TDC

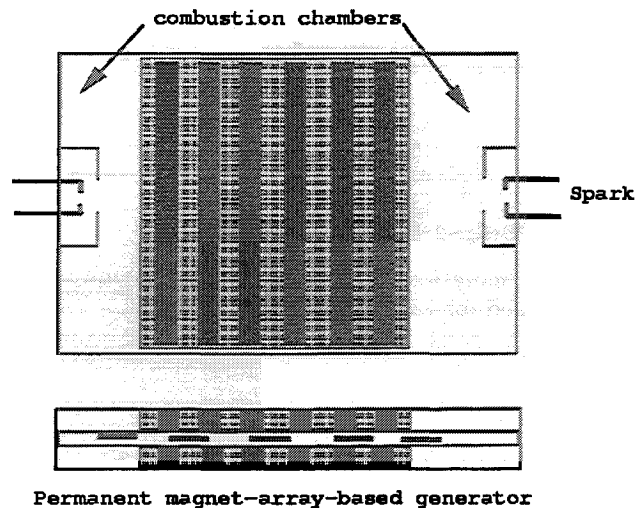


**Fig. 1 The dual-combustor micro-engine with magnetic array.**

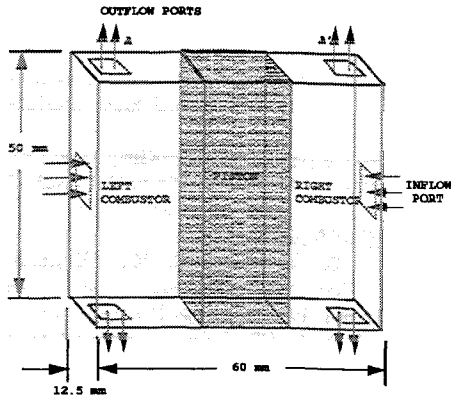


Fig. 2 Schematic of a dual-combustor model used for LES.

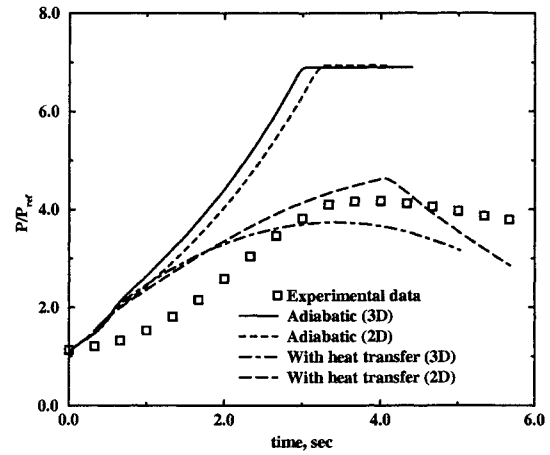


Fig. 5 Effect of heat transfer on the peak pressure reached in a constant volume combustor.

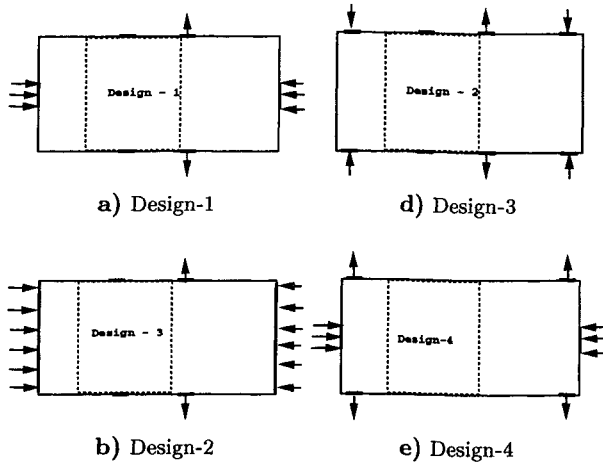


Fig. 3 Schematics of the different dual-combustor designs used for LES

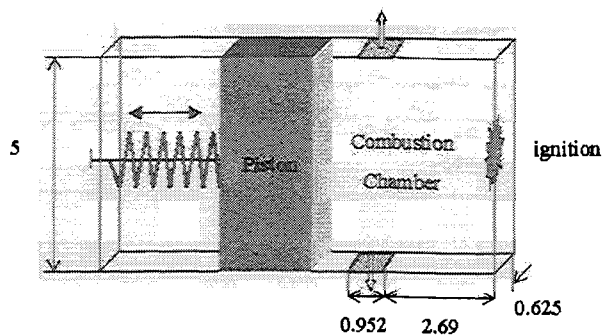


Fig. 4 Schematic of the single-combustor design. The second combustor is replaced by a spring in this design. All dimensions are in cm.

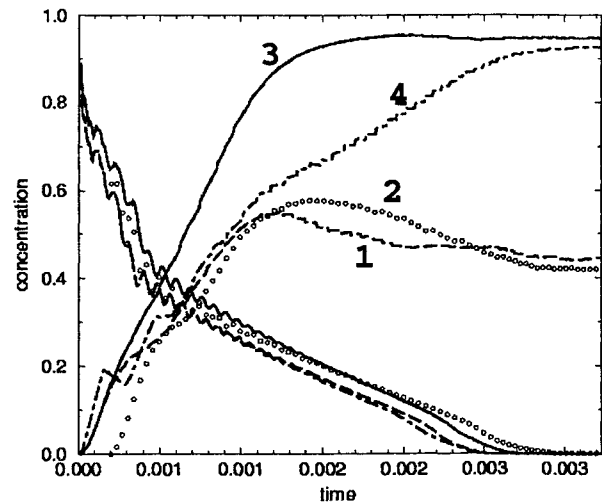
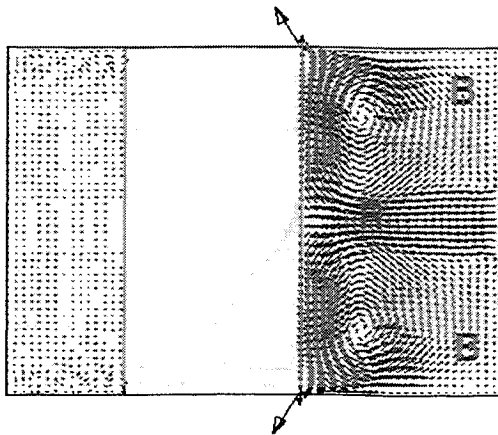
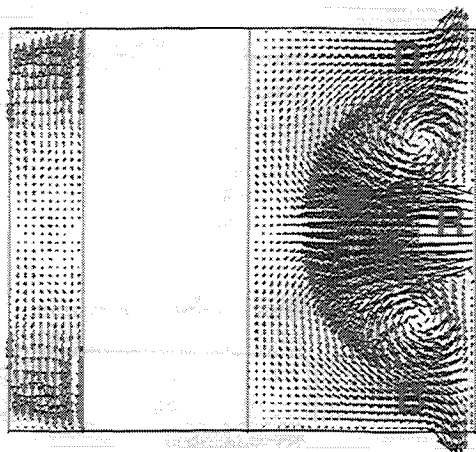


Fig. 6 Variation of reactant concentration in the combustion chamber with injection for the various designs. Clearly, Designs 1 and 2 fail to reach sufficient concentration level before ignition and thus, fails.

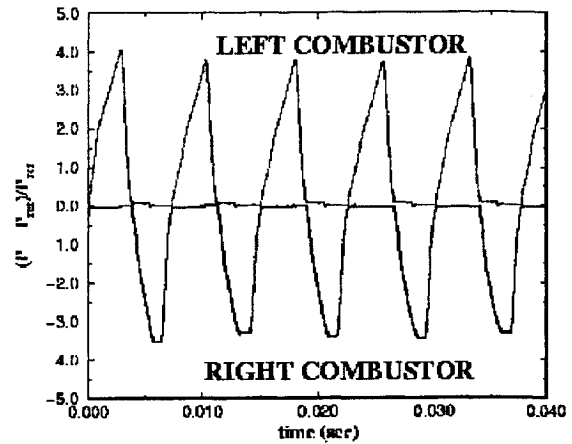


a) Design-1

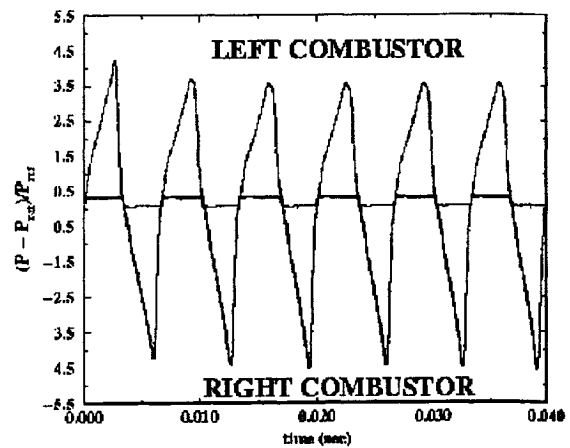


b) Design-4

**Fig. 7** Velocity vector field for designs 1 and 4. Trapped burnt products (marked by letter B) from the previous cycle in Design-1 limits the magnitude of the reactant (marked by letter R) concentration reached at end of the injection period.

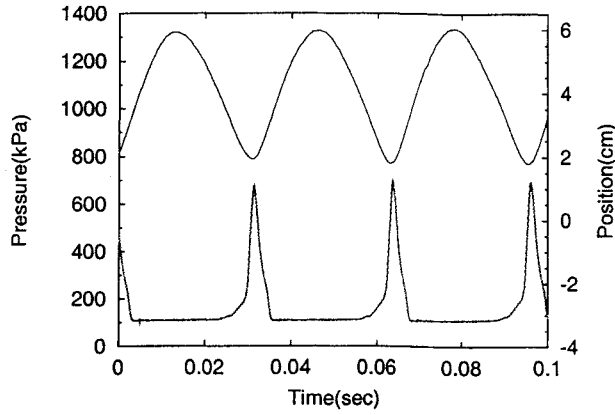


a) Two-Dimensional Simulation

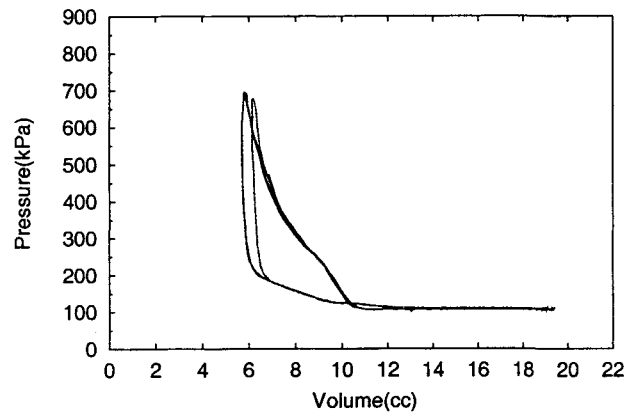


b) Three-Dimensional Simulations

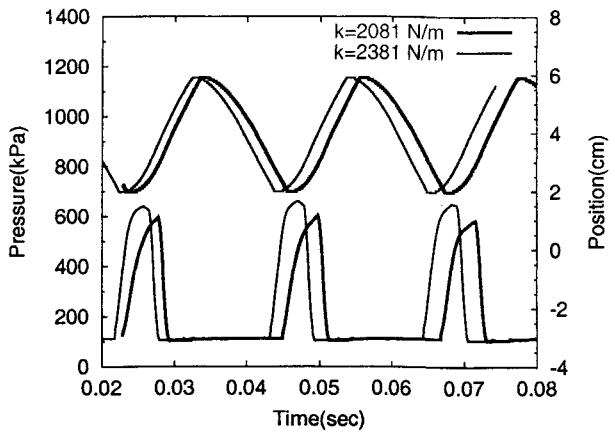
**Fig. 8** Pressure oscillations in Design-4. Both combustors achieve identical oscillation amplitude and frequency and there are many similarities between the 2D and 3D results.



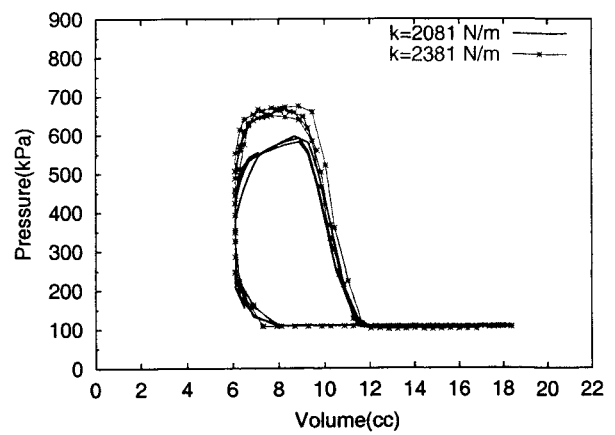
a) Experiment



a) Experiment



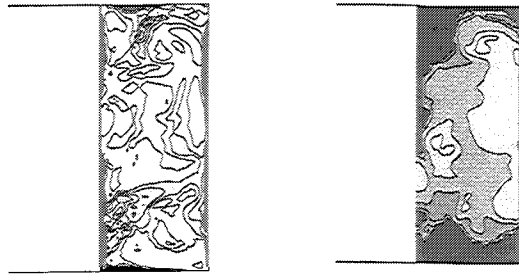
b) Numerical



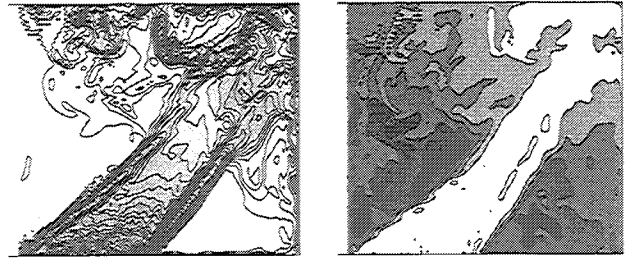
b) Numerical

**Fig. 9** Experimental and numerical results for the pressure oscillation and piston stroke motion in the single-combustor device.

**Fig. 10** Experimental and numerical results for the pressure-volume variation in the single-combustor device.



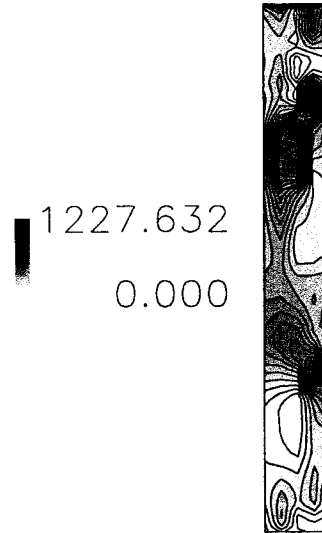
a) Subgrid kinetic energy      b) Temperature



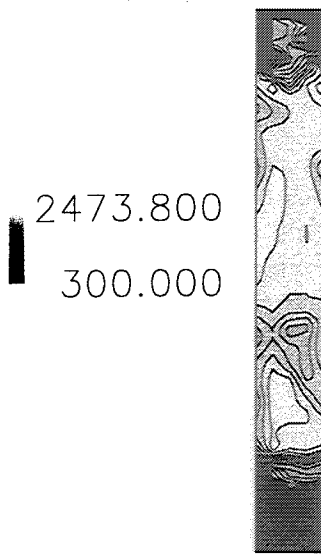
a) Subgrid kinetic energy      b) Temperature



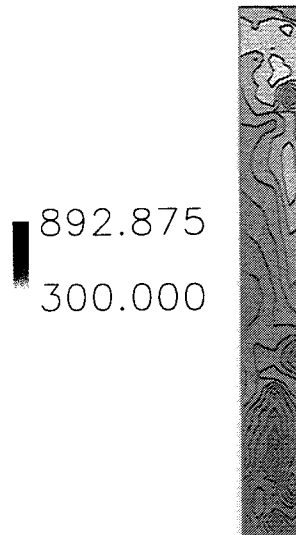
c) Subgrid kinetic energy(spanwise)



c) Subgrid kinetic energy(spanwise)



d) Temperature(spanwise)



d) Temperature(spanwise)

**Fig. 11 Subgrid kinetic energy and temperature contours at ignition.**

**Fig. 12 Subgrid kinetic energy and temperature contours at injection.**